Ionization Waves of Arbitrary Velocity

D. Turnbull, P. Franke, J. Katz, J. P. Palastro, I. A. Begishev, R. Boni, J. Bromage, A. L. Milder, J. L. Shaw, and D. H. Froula

Phys. Rev. Lett. **120**, 225001 — Published 31 May 2018
DOI: 10.1103/PhysRevLett.120.225001

Ionization Waves of Arbitrary Velocity

D. Turnbull,[1, *] P. Franke,[1, 2] J. Katz,[1, 3] J. P. Palastro,[1, 3] I. A. Begishev,[1, 3]
R. Boni,[1, 3] J. Bromage,[1, 3] A. L. Milder,[1, 2] J. L. Shaw,[1] and D. H. Froula[1, 2]
[1] *University of Rochester Laboratory for Laser Energetics, 250 E River Rd., Rochester, NY 14623, USA*
[2] *University of Rochester Department of Physics & Astronomy, B&L Hall, Rochester, NY 14627, USA*
[3] *University of Rochester Institute of Optics, 480 Intercampus Drive, Rochester, NY 14627, USA*

(Dated: Thursday 3rd May, 2018)

Flying focus is a technique that uses a chirped laser beam focused by a highly chromatic lens to produce an extended focal region within which the peak laser intensity can propagate at any velocity. When that intensity is high enough to ionize a background gas, an ionization wave will track the intensity isosurface corresponding to the ionization threshold. We report on the demonstration of such ionization waves of arbitrary velocity. Subluminal and superluminal ionization fronts were produced that propagated both forward and backward relative to the ionizing laser. All backward and all superluminal cases mitigated the issue of ionization-induced refraction that typically inhibits the formation of long, contiguous plasma channels.

Efforts to engineer plasmas for the generation and manipulation of electromagnetic waves have been growing in sophistication. Recent examples of plasma-based photonic devices include mirrors [1–3], wave plates [4, 5], polarizers [6, 7], q−plates [8], radiation sources ranging from x-rays [9, 10] to THz [11, 12], laser amplifiers [13–15], and laser compressors [16]. Many such tools rely on the controlled propagation of an ionization front, the velocity of which can strongly impact the performance of the system.

For example, light propagating within an ionization front will undergo "photon acceleration"—a continual upshift of its frequency induced by the dynamic refractive index gradient [17–20]. However, the frequency upshift results in group velocity acceleration and a tendency for the source to decouple from the constant velocity ionization front. To highlight a second example, recent simulations of plasma-based laser amplification showed that a dynamic ionization front propagating just ahead of an amplifying seed pulse provides enhanced control over plasma parameters as well as improved noise suppression [21].

A technique providing unprecedented spatiotemporal control over the propagation of laser intensity—the "flying focus"—was recently pioneered[22, 23]. A chirped broadband laser pulse with duration τ (with the sign of τ indicating the direction of the chirp) is focused by a highly chromatic diffractive optic that produces an extended focal region with length l. In general, each color reaches best focus at a unique time, and the rate at which the location of best focus moves is uniquely determined by the ratio τ/l for a linearly chirped beam. By tuning τ/l, peak laser intensity can be made to propagate at any velocity, from $-\infty$ to $+\infty$.

Subsequent calculations have demonstrated that a dynamic ionization front will track the velocity of an intensity isosurface at the ionization threshold of a background gas [24]. Therefore, the flying focus can be used to produce an ionization wave of arbitrary velocity (IWAV). These simulations also revealed that backward IWAV propagation relative to the ionizing laser mitigates ionization-induced refraction, which typically degrades the formation of long, uniform, laser-produced plasmas [25, 26].

In this Letter, we report the first experimental demonstration of ionization waves of arbitrary velocity. The velocities ranged from subluminal to superluminal (slower and faster than the speed of light, respectively), both forward- and backward-propagating relative to the ionizing laser. Ionization fronts were observed to propagate smoothly over several millimeters in most cases, although subluminal forward propagation was degraded by ionization-induced refraction, as expected. To diagnose the IWAV propagation, a novel spectrally resolved schlieren diagnostic was developed, exploiting the linear time-frequency relationship of a chirped probe. These data demonstrate the feasibility of flying-focus–produced IWAV's for use in applications like those discussed above.

The experimental setup is shown in Fig. 1. An Nd:YLF laser with optical chirped-pulse parametric amplification (OPCPA) generated a beam with central wavelength $\lambda_0 = 1.053$ μm and full-width half-maximum (FWHM) bandwidth $\Delta\lambda = 8.7$ nm, providing the source for the pump and probe beams. The power spectrum was very flat (SG8), generating a square temporal profile when the laser was chirped to durations much longer than its transform limit. The linear chirp was adjusted using the grating position in the stretcher. A beamsplitter directed 85% of the energy to the pump path. A diffractive lens with radially varying groove density, described more fully in Ref. [23], was used to focus the pump beam in air at atmospheric pressure. Its focal length for the central wavelength of the pump was $f_0 = 51.1$ cm, and it produced an extended focal region of length $l = f_0\Delta\lambda/\lambda_0 = 4.2$ mm, with the red and blue sides of the spectrum focusing nearest to and furthest from the lens, respectively. With an energy of 25.5 ± 0.3 mJ, the pump created a plasma channel in air at best focus

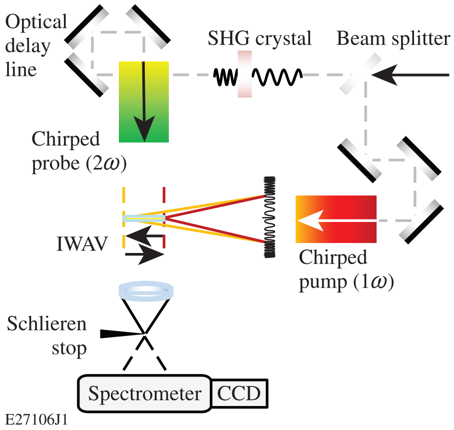

FIG. 1. A 1.053-μm laser with tunable pulse duration τ was split into two beams. The pump beam remained 1ω and was focused by a diffractive optic to produce an ionization wave of arbitrary velocity (IWAV). The probe beam was converted to 2ω and diagnosed the plasma channel in a side-on geometry coincident with the plasma formation. A spectrally resolved schlieren diagnostic was used to determine the ionization front velocity.

(a) Flying focus velocity

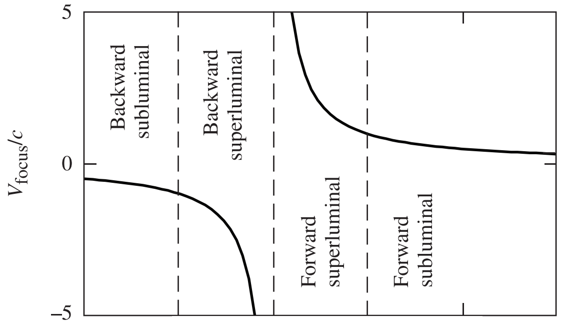

(b) Chirped schlieren slope

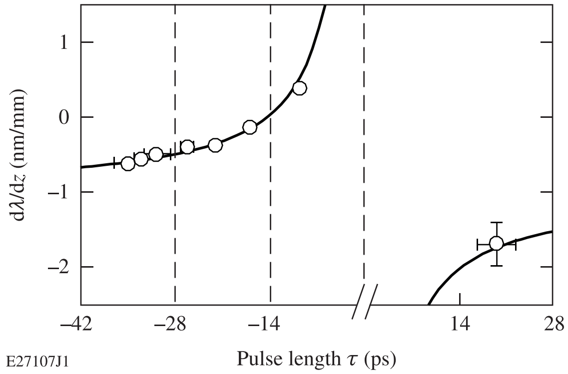

FIG. 2. (a) The flying focus velocity (i.e., the speed at which constant intensity isosurfaces move near best focus) is determined by the ratio of the chirped pulse duration to the length of the extended chromatic focal region produced by the diffractive optic. Any velocity (including faster than the speed of light) is achievable in both the forward and backward directions relative to the laser propagation. (b) For the spectrally resolved schlieren diagnostic, the expected linear slope of an edge marking the onset of plasma formation is plotted as a function of pump and probe pulse duration. The overlaid points correspond to the experimental data. Both forward- and backward-propagating ionization waves of arbitrary velocity were produced, with velocities both less than and greater than the speed of light in each direction.

for pulse durations ranging from best compression (< 1 ps) up to ≈ 40 ps. With 99% efficiency into the first order and a minimally-aberrated beam profile at best focus ($14 \times 18 \mu$m FWHM —better than twice the diffraction limit—as shown in the supplementary material of Ref. [23]), a typical (e.g., for a 26 ps pulse duration) intensity at best focus was $\approx 5 \times 10^{14}$ W/cm^2. This seems high by a factor of $\approx 5-10$ compared to ionization thresholds quoted in the literature [27], but no attempt was made in this experiment to minimize the energy in order to identify an ionization threshold; furthermore, the threshold has a strong pulse length dependence in this regime [27, 28], and with flying focus it is unclear whether to use the nominal pulse length or an effective pulse duration for the dynamic laser intensity peak.

The additional 15% transmitted through the beamsplitter was down-collimated, converted to 2ω using a second harmonic crystal, and directed to the plasma orthogonal to the pump axis for use as a probe beam. An optical delay path was used to time the probe such that its passage coincided with the IWAV propagation. The plasma channel was imaged along the probe path onto the entrance slit of a 0.3-m imaging spectrometer equipped with a 1200 grooves/mm grating. A knife edge was used as a schlieren stop in a focal location of the probe beam along the imaging path. It was oriented in order to probe gradients orthogonal to the axis of the plasma channel (i.e., the edge of the channel). A Finger Lakes CCD camera was used to capture images at the exit plane of the spectrometer.

Removing the schlieren stop, opening the spectrometer slit, and operating the spectrometer in zero order, the CCD camera captured 2-D shadowgraphy images of the plasma channels. Inserting the schlieren stop with otherwise the same parameters yielded 2-D schlieren images. The spectrometer slit was then centered on the edge of the plasma channel (the location of maximum signal) and the grating was set to disperse the probe wavelengths orthogonal to the plasma channel axis. The spectral axis effectively provides picosecond time resolution due to the linear time-frequency dependence of the chirped probe beam.

The ionization front velocity [Fig. 2(a)] is dictated by the focal-spot velocity [24], which was given in Ref. [23] and is briefly rederived here. The instantaneous focal-spot velocity is $v_f(z) = \frac{dz}{dt}$ where dz is the distance between the focal locations of two colors and dt is the difference in their arrival times at best focus. Since the laser chirp is fixed in a reference frame moving with the laser, it is convenient to define $\xi = t - z/c$, in which case the focal-spot velocity $v_f(z) = \frac{dz}{d\lambda}\frac{d\lambda}{d\xi}\frac{d\xi}{dt}$ is related to the longitudinal spatial dispersion $\frac{dz}{d\lambda}$ and the chirp $\frac{d\lambda}{d\xi}$. With some algebra, the formula becomes $v_f(z) = c(1 + c\frac{d\xi}{d\lambda}\frac{d\lambda}{dz})^{-1}$. For linear spatial dispersion $\frac{d\lambda}{dz} = -\lambda_0/f_0$ from the diffractive lens and a linear chirp much longer than the transform-limited pulse duration $\frac{d\xi}{d\lambda} = -\tau/\Delta\lambda$ (i.e., the FWHM spectral bandwidth is spread out over the FWHM pulse duration), the focal-spot velocity is constant and simplifies to $v_f = c(1 + \tau c/l)^{-1}$. Negative values of τ correspond to negatively chirped beams, with the blue end of the spectrum preceding the red end in time. The IWAV velocity is converted to an observable on the spectrally resolved schlieren measurement by noting that $\frac{dz}{dt} = \frac{dz}{d\lambda}\frac{d\lambda}{dt}$, and $\frac{d\lambda}{dt} = -\Delta\lambda/2\tau$ for the linearly chirped second harmonic probe beam. Therefore, the expected edge slope on the schlieren diagnostic [Fig. 2(b)] is given by $\frac{d\lambda}{dz} = -\frac{\Delta\lambda}{2}\left(\frac{1}{c\tau} + \frac{1}{l}\right)$.

Results from the spectrally resolved schlieren diagnostic are shown in Fig. 3. Each image is an average of five to ten shots divided by an average of several reference spectra, which were obtained by removing the schlieren stop and blocking the pump beam. The pump beam propagated from left to right along the z axis. An edge-finding routine was used to find the time of the ionization wave's appearance at each axial location; vertical lineouts were taken averaging over ≈ 30-μm increments along the z axis, and typically the value closest to 10% along the spectral axis was specified as the edge (note that slight variation in signal levels between cases resulted from differences in plasma channel alignment to the spectrometer slit and schlieren stop positioning). The slope was determined from a linear best fit through the data points. The points found by the edge-finding routine, as well as the best fit result, are plotted with the data in Fig. 3.

In Figs. 3(a)-3(c), there is no signal on the blue side of the probe spectrum because that portion of the probe passed the pump's focal region prior to any plasma formation. The edge of the signal then appears and varies linearly, as expected, over a distance of at least 2 to 3 mm. Hydrodynamic expansion of the plasma channel is negligible on the time scale of the probe beam, so the plasma channel persists and continues to refract all subsequent probe colors on the red side of the spectrum. Figures 3(a) and 3(b) are both examples of superluminal backward propagation since $-2l/c < \tau < -l/c$; the latter example is close to $\tau = -l/c$, in which case each color arrives at best focus simultaneously and the IWAV travels across the focal region instantaneously.

(a) τ ≈ −22 ps, superluminal backward propagation

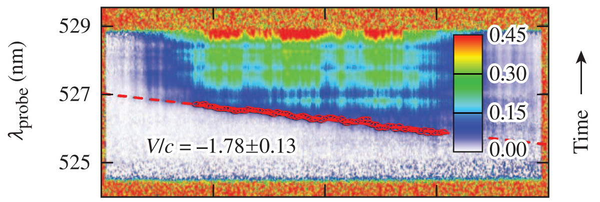

(b) τ ≈ −17 ps, nearly instantaneous line focus

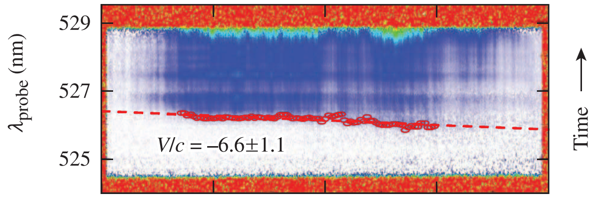

(c) τ ≈ −10 ps, superluminal forward propagation

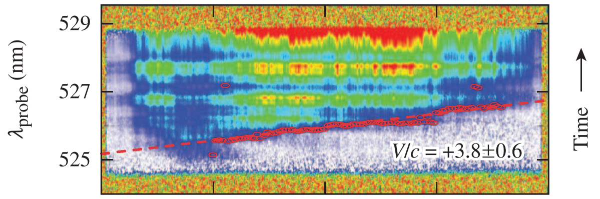

(d) τ ≈ +20 ps, subluminal forward propagation

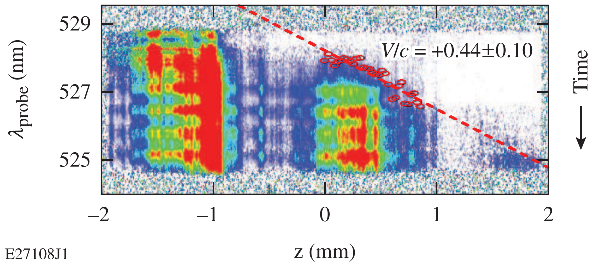

FIG. 3. Spectrally resolved schlieren results. (a) An example of superluminal backward propagation for $\tau \approx -22$ ps. The probe is negatively chirped so the direction of time is from the blue end to the red end of the spectrum. The IWAV begins at $+z$ and propagates backward to $-z$ along the pump axis. (b) A more highly superluminal example producing a nearly instantaneous line focus. (c) With $-l/c < \tau < 0$, the IWAV remains superluminal but switches to forward-propagating, reversing the sign of the slope. (d) When the probe is positively chirped, the direction of time is effectively reversed, and subluminal forward propagation produces a disjointed plasma channel because of ionization-induced refraction.

Figure 3(c) shows an example of superluminal forward propagation, with $-l/c < \tau < 0$. Note that although the IWAV copropagates with the ionizing laser, ionization-induced refraction did not compromise the channel formation. This naturally follows from the fact that the shorter wavelength photons that ionize the plasma at larger values along the z axis are ahead of the ionization front and are therefore not affected by propagation through the existing plasma. (Similar logic explains why superluminal IWAV propagation does not violate causality.)

In Fig. 3(d), the laser is positively chirped, which always yields a subluminal forward-propagating flying focus. Note that the sign of the slope expected in the schlieren images is the same as for negatively chirped

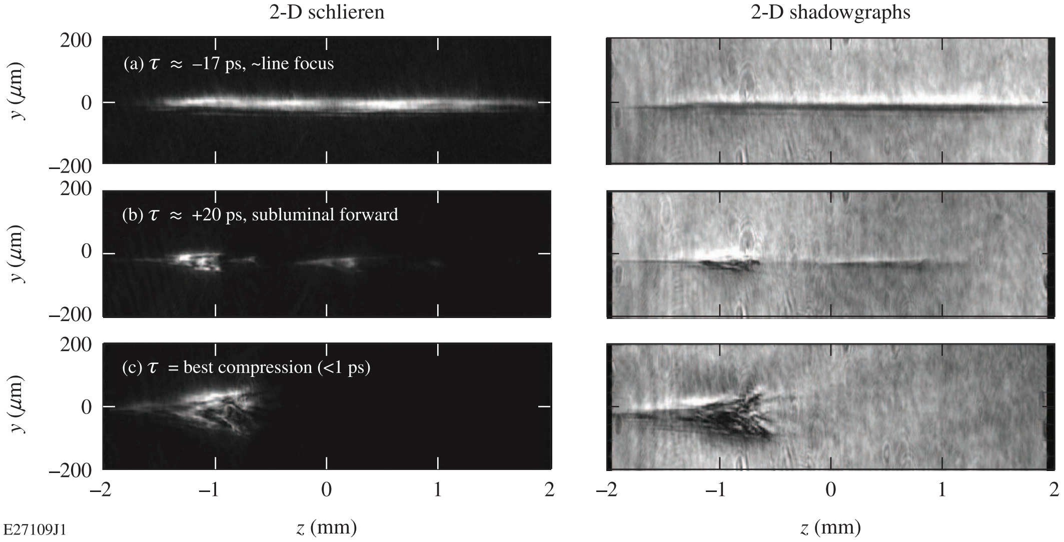

FIG. 4. Two-dimensional schlieren and shadowgraphy of various cases. (a) The $\tau \approx -17$ ps example shows a long, uniform plasma channel and is representative of all tested cases of backward propagation as well as superluminal forward propagation. (b) Subluminal forward propagation leads to plasma channel breakup because of ionization-induced refraction; (c) this also occurs for best compression, which is most similar to conventional beam propagation in that laser intensity moves forward at the group velocity.

backward propagation because two sign changes (the IWAV propagation direction and the direction of the probe chirp) cancel one another out; only within the narrow range $-l/c < \tau < 0$ is the slope positive because the IWAV's are forward-propagating but the probe chirp is negative [e.g., Fig. 3(c)]. The reversed direction of time is evident in the schlieren image because the blue side of the spectrum probes the fully formed plasma channels in contrast to the previous examples. Note also that for $\tau > -l/(2c)$, the time v_f/l that it takes the IWAV to propagate from one edge of the focal region to the other is greater than the probe pulse duration $|\tau|$, limiting the IWAV propagation distance that the probe can diagnose. Therefore, in the example shown, the plasma is already over 1 mm in length by the time the probe arrives.

The key difference in Fig. 3(d) is that the schlieren signal appears disjointed along the axis of the pump beam. This results from ionization-induced refraction in the case of subluminal forward propagation—an effect that was predicted in Ref. [24]. To illustrate this more clearly, 2-D shadowgraphs and 2-D schlieren images are shown for three cases in Fig. 4. The example in Fig. 4(a) happens to be the case of a nearly instantaneous line focus, but all cases of backward propagation that were tested, in addition to superluminal forward propagation, produced similar long, uniform plasma channels. Contrast that with Fig. 4(b), which shows that the initial plasma at $z = -1$ mm disrupts subsequent plasma formation over the next ≈ 1 mm. At a later point along the pump axis, the initial plasma is far enough away (refracting a small enough fraction of the wavelength that focuses to that location) that ionization is once again triggered locally. This cycle repeats itself once more, producing three distinct sparks [the third being more evident in Fig. 3(d) than in Fig. 4(b)].

Using the edge-finding routine on the middle spark resulted in a linear fit that roughly tracks the central plasma and also seems to predict the timing of the third plasma's formation, but the fit's confidence was much lower, resulting in larger error bars. The slopes for all data sets, including subluminal backward propagation (which has not been shown), were overplotted with the analytic calculation in Fig. 2(b). Pulse durations were measured using an ultrafast streaked spectrometer [29] for the second harmonic probe beam and two autocorrelators for the fundamental beam (the three diagnostics agreed to within 1 to 2 ps). In most cases, the uncertainties in pulse length and schlieren slope were smaller than the marker size shown, with the exception of the subluminal forward-propagating IWAV just described; nevertheless, that result is also in good agreement with the prediction.

For completeness, Fig. 4(c) shows the plasma channel formation that occurs when the probe duration was at best compression ($\tau \approx 500$ fs). In this case, the diffractive lens produces a distributed focal spot that would be expected to have approximately constant intensity over several millimeters while propagating at the laser's group velocity (and is thus the case most similar to conventional beam propagation). This case was degraded even more severely by ionization-induced refraction such that only one short plasma was formed.

In summary, ionization waves of arbitrary velocity have been demonstrated experimentally using the flying focus. While superluminal ionization front propagation has been demonstrated previously [30], and a different (more complicated) scheme for tuning the velocity of ionization waves has been proposed [31], to our knowledge this represents the first experimental demonstration of IWAV's. Producing plasma channels in this manner could facilitate improved performance in a wide range of applications that rely on synchonization with an ionization front, such as plasma-based laser amplification, photon acceleration, and THz generation. Even neglecting the potentially beneficial dynamics of the ionization front, we have demonstrated long, uniform, flying focus-produced plasma channels that are comparable to those created using an axicon lens, which may be of interest to applications that utilize plasma waveguides [32–35].

This work was supported by the U.S. Department of Energy Office of Fusion Energy Sciences under contract No. DE-SC0016253, Department of Energy under Cooperative Agreement No. DE-NA0001944, the University of Rochester, and the New York State Energy Research and Development Authority. The support of DOE does not constitute an endorsement by DOE of the views expressed in this article.

---

[*] turnbull@lle.rochester.edu

[1] C. Thaury, F. Quere, J.-P. Geindre, A. Levy, T. Ceccotti, P. Monot, M. Bougeard, F. Reau, P. d'Oliveira, P. Audebert, R. Marjoribanks, and P. Martin, Nat. Phys. **3**, 424 (2007).

[2] S. Monchocé, S. Kahaly, A. Leblanc, L. Videau, P. Combis, F. Réau, D. Garzella, P. D'Oliveira, P. Martin, and F. Quéré, Phys. Rev. Lett. **112**, 145008 (2014).

[3] G. Lehmann and K. H. Spatschek, Phys. Rev. Lett. **116**, 225002 (2016).

[4] P. Michel, L. Divol, D. Turnbull, and J. D. Moody, Phys. Rev. Lett. **113**, 205001 (2014).

[5] D. Turnbull, P. Michel, T. Chapman, E. Tubman, B. B. Pollock, C. Y. Chen, C. Goyon, J. S. Ross, L. Divol, N. Woolsey, and J. D. Moody, Phys. Rev. Lett. **116**, 205001 (2016).

[6] D. J. Stark, C. Bhattacharjee, A. V. Arefiev, T. Toncian, R. D. Hazeltine, and S. M. Mahajan, Phys. Rev. Lett. **115** (2015).

[7] D. Turnbull, C. Goyon, G. E. Kemp, B. B. Pollock, D. Mariscal, L. Divol, J. S. Ross, S. Patankar, J. D. Moody, and P. Michel, Phys. Rev. Lett. **118**, 015001 (2017).

[8] K. Qu, Q. Jia, and N. J. Fisch, Phys. Rev. E **96**, 053207 (2017).

[9] M. R. Edwards and J. M. Mikhailova, Phys. Rev. Lett. **117**, 125001 (2016).

[10] M. R. Edwards, J. M. Mikhailova, and N. J. Fisch, Phys. Rev. E **96**, 023209 (2017).

[11] C. D'Amico, A. Houard, M. Franco, B. Prade, A. Mysyrowicz, A. Couairon, and V. T. Tikhonchuk, Phys. Rev. Lett. **98**, 235002 (2007).

[12] K. Y. Kim, J. H. Glownia, A. J. Taylor, and G. Rodriguez, Opt. Express **15**, 4577 (2007).

[13] G. Shvets, N. J. Fisch, A. Pukhov, and J. Meyer-ter Vehn, Phys. Rev. Lett. **81**, 4879 (1998).

[14] L. Lancia, A. Giribono, L. Vassura, M. Chiaramello, C. Riconda, S. Weber, A. Castan, A. Chatelain, A. Frank, T. Gangolf, M. N. Quinn, J. Fuchs, and J.-R. Marquès, Phys. Rev. Lett. **116**, 075001 (2016).

[15] R. K. Kirkwood, D. P. Turnbull, T. Chapman, S. C. Wilks, M. D. Rosen, R. A. London, L. A. Pickworth, W. H. Dunlop, J. D. Moody, D. J. Strozzi, P. A. Michel, L. Divol, O. L. Landen, B. J. MacGowan, B. M. Van Wonterghem, K. B. Fournier, and B. E. Blue, Nat. Phys. **14**, 80+ (2018).

[16] V. M. Malkin, G. Shvets, and N. J. Fisch, Phys. Rev. Lett. **82**, 4448 (1999).

[17] W. B. Mori, Physical Review A **44**, 5118 (1991).

[18] E. Esarey, G. Joyce, and P. Sprangle, Physical Review A **44**, 3908 (1991).

[19] P. Sprangle and E. Esarey, Phys. Fluids B **4**, 2241 (1992).

[20] J. M. Dias, C. Stenz, N. Lopes, X. Badiche, F. Blasco, A. Dos Santos, L. Oliveira e Silva, A. Mysyrowicz, A. Antonetti, and J. T. Mendonça, Physical Review Letters **78**, 4773 (1997).

[21] D. Turnbull, S. Bucht, A. Davies, D. Haberberger, T. Kessler, J. L. Shaw, and D. H. Froula, Phys. Rev. Lett. **120**, 024801 (2018).

[22] A. Sainte-Marie, O. Gobert, and F. Quéré, Optica **4**, 1298 (2017).

[23] D. H. Froula, D. Turnbull, T. Kessler, D. Haberberger, S.-W. Bahk, I. A. Begishev, R. Boni, S. Bucht, A. Davies, J. Katz, and J. L. Shaw, Nat. Phot. **12**, 262 (2018).

[24] J. P. Palastro, D. Turnbull, S.-W. Bahk, R. K. Follett, J. L. Shaw, D. Haberberger, J. Bromage, and D. H. Froula, Phys. Rev. A **97**, 033835 (2018).

[25] W. P. Leemans, C. E. Clayton, W. B. Mori, K. A. Marsh, P. K. Kaw, A. Dyson, C. Joshi, and J. M. Wallace, Phys. Rev. A **46**, 1091 (1992).

[26] T. M. Antonsen and Z. Bian, Phys. Rev. Lett. **82**, 3617 (1999).

[27] C. G. Morgan, Rep. Prog. Phys. **38**, 621 (1975).

[28] W. E. Williams, M. J. Soileau, and E. W. V. Stryland, Appl. Phys. Lett. **43**, 352 (1983).

[29] J. Katz, R. Boni, R. Rivlis, C. Muir, and D. H. Froula, Rev. Sci. Instrum. **87**, 11E535 (2016).

[30] I. Alexeev, K. Y. Kim, and H. M. Milchberg, Phys. Rev. Lett. **88**, 073901 (2002).

[31] A. Zhidkov, T. Esirkepov, T. Fujii, K. Nemoto, J. Koga, and S. V. Bulanov, Phys. Rev. Lett. **103**, 215003 (2009).

[32] C. G. Durfee and H. M. Milchberg, Phys. Rev. Lett. **71**, 2409 (1993).

[33] P. Volfbeyn, E. Esarey, and W. P. Leemans, Phys. Plasmas **6**, 2269 (1999).

[34] Y.-F. Xiao, H.-H. Chu, H.-E. Tsai, C.-H. Lee, J.-Y. Lin, J. Wang, and S.-Y. Chen, Phys. Plasmas **11**, L21 (2004).

[35] S. Z. Green, E. Adli, C. I. Clarke, S. Corde, S. A. Edstrom, A. S. Fisher, J. Frederico, J. C. Frisch, S. Gessner, S. Gilevich, P. Hering, M. J. Hogan, R. K. Jobe, M. Litos, J. E. May, D. R. Walz, V. Yakimenko, C. E. Clayton, C. Joshi, K. A. Marsh, N. Vafaei-Najafabadi, and P. Muggli, Plas. Phys. & Cont. Fus. **56**, 084011 (2014).